IEEE Access
Multidisciplinary ⋮ Rapid Review ⋮ Open Access Journal

Received 4 March 2024, accepted 12 March 2024, date of publication 18 March 2024, date of current version 26 March 2024.

Digital Object Identifier 10.1109/ACCESS.2024.3379011

RESEARCH ARTICLE

Performance Analysis of BLE-5.1 Angle of Arrival Estimation Using Embedded Radiation Patterns on a 3 × 3 Uniform Rectangular Array

OTTAVIO CRISAFULLI[1,2], NICOLÒ IVAN PIAZZESE[3], SANTI CONCETTO PAVONE[1,4], (Senior Member, IEEE), GIUSEPPE GIAMMELLO[1,4], GIOVANNI GALVAGNA[3], SALVATORE PITRULLI[3], ANDREA FRANCESCO MORABITO[1,2], (Senior Member, IEEE), LORETO DI DONATO[1,4], (Senior Member, IEEE), MICHELE SARDO[3], AND GINO SORBELLO[1,4], (Member, IEEE)

[1]Consorzio Nazionale Interuniversitario per le Telecomunicazioni (CNIT), Research Unit, University of Catania, 95125 Catania, Italy
[2]Department of Information Engineering, Infrastructure and Sustainable Energy (DIIES), Mediterranea University of Reggio Calabria, 89122 Reggio Calabria, Italy
[3]STMicroelectronics Catania, 95121 Catania, Italy
[4]Dipartimento di Ingegneria Elettrica, Elettronica e Informatica (DIEEI), University of Catania, 95123 Catania, Italy

Corresponding author: Santi Concetto Pavone (santi.pavone@unict.it)

The work of Ottavio Crisafulli, Loreto Di Donato, and Gino Sorbello was supported by the European Union through the Italian National Recovery and Resilience Plan (NRRP) of NextGenerationEU, partnership on "Telecommunications of the Future," under Grant PE0000001—Program RESTART. The work of Santi Concetto Pavone and Giuseppe Giammello was supported by European Union (NextGeneration EU) through the NRRP Project SAMOTHRACE under Grant ECS00000022.

ABSTRACT The introduction of new Direction finding (DF) features in Bluetooth Low Energy (BLE) 5.1, has brought about new hardware design requirements for locators. These requirements include the ability to support accurate and fast direction-finding algorithms while maintaining compactness. To address these needs, a uniform rectangular antenna array with octagonal patches has been chosen. The single antenna features a Circular Polarized (CP) Bandwidth (BW) of 3.1% for a 6-dB threshold and a CP BW of 1.59% for a 3-dB threshold. Different antenna array configurations have been compared in terms of the inter-element distance of the radiators to find a balance between antenna miniaturization and accuracy. From this analysis, an array antenna prototype (i.e., locator BLE) has been manufactured. In this paper, we analyze the performance of Direction of Arrival (DoA) estimation in BLE by comparing the Conventional Steering Vector (CSV) approach with a new Embedded Radiation Pattern (ERP) approach, which takes into account mutual coupling effects and gain loss due to miniaturization. The Mean Absolute Error (MAE) served as the performance metric to assess the accuracy of the main DoA detection. ERP outperforms CSV, in no-loss and multi-path scenarios. Numerical simulations show that ERP offers higher accuracy (lower MAE over θ and ϕ) when the number of snapshots increases. Performance evaluation for MUltiple SIgnal Classification (MUSIC) and Bartlett algorithms highlights that for a SNR $>$ 20 dB, the accuracy does not depend on the number of snapshots used and faster computation is achieved for a single snapshot.

INDEX TERMS Angle of arrival (AoA), direction finding (DF), direction of arrival (DoA), Bluetooth low energy (BLE), Bartlett, multiple signal classification (MUSIC), conventional steering vector (CSV), embedded radiation pattern (ERP), patch antenna array, uniform rectangular array (URA), mutual coupling (MC).

I. INTRODUCTION

Bluetooth Low Energy (BLE) 5.1, introduced new possibilities for indoor positioning applications since it offers the Direction Finding (DF) feature, including Angle of

The associate editor coordinating the review of this manuscript and approving it for publication was Hussein Attia.

Arrival (AoA) and Angle of Departure (AoD) schemes, by adopting multiple antennas in the receiver architecture (i.e., locator) and a single antenna for the transmitter (i.e, tag).

At the state of art, the most used DoA algorithms are MUltiple SIgnal Classification (MUSIC) and Bartlett. Both require, as first step, the estimation of the covariance matrix. MUSIC, starting from this matrix, estimates the eigenvectors of the noise space and through these constructs a function, which in the case of rectangular arrays, is two-dimensional, known as the pseudo-spectrum function (PSF). Bartlett from the covariance matrix also constructs a PSF, with a lower resolution than Schmidt's MUSIC algorithm [1].

An alternative approach to DF is the Orthogonal Matching Pursuit (OMP) algorithm, which leverages the sparsity of incoming signals within a redundant dictionary to reconstruct the sparse representation of the received data [2]. From this sparse representation, the incoming signals can be recovered.

Moreover, in [3] an on-grid sparse recovery algorithm with a discrete subset of DoAs is considered for signal estimation and related Angle of Arrival (AoA) finding. The estimated signal is obtained as a linear combination of the columns of the dictionary interested in the sparse signal reconstruction. The main drawback of OMP algorithms is the difficulty of resolving DoAs when the sources are very close.

Focused Orthogonal Matching Pursuit (FOMP) algorithm [4] is an improved version that can detect peaks from the angular spectrum even for two adjacent incoming signal sources. Most of these algorithms have been adopted for Uniform Linear Array (ULA) configurations. Nevertheless, by considering non-uniform arrays a higher DoA resolution is achieved at the expense of phase ambiguity when the inter-element distance of radiators is greater than $\frac{\lambda}{2}$ [5].

In [6], OMP applied to a Hybrid non-uniform array configuration (HOMP) consisting of two uniform linear sub-arrays with different inter-spacing between elements is able to obtain higher accuracy with respect to OMP and FOMP, thus avoiding phase ambiguity. These algorithms have been studied as 2D problems considering incoming sources only in the elevation plane. An extended version of OMP performing over azimuth and elevation angles has been designed in the 3D-OMP and 3D-FOMP [7].

Finally, in [8], the estimation performances of the subspace-based algorithms and Compressive sensing-based methods have been combined. From this analysis it has been inferred that subspace-based methods, like 3D-MUSIC and 3D-ESPRIT [9], have better angular resolution with respect to Compressive sensing methods for small array configurations and a higher number of snapshots; when the array becomes large, Compressive-sensing performs better.

In this work, we consider a circularly polarized (CP) uniform rectangular array operating in the BLE frequency range [2.40 − 2.48] GHz. The single elements of the array consist of octagonal patches arranged in a 3×3 configuration, with a normalized spacing distance $\overline{d} = \frac{d}{\lambda}$ of [0.5, 0.4, 0.33]. We propose the use of circular polarization for both the tag and locator. Circular polarization has been shown to provide immunity to signal degradation caused by bad weather conditions and is less affected by the relative orientation between the transmitting and receiving antennas [10], [11]. After providing a brief overview of the mathematical model used in the DF scheme, we compare the performance of the MUSIC and Bartlett algorithms for different locator sizes. Once the optimal array configuration has been selected, we conduct a thorough comparison between the conventional steering vector (CSV) approach and the newly proposed method that employs simulated or measured embedded radiation patterns (ERPs). In addition, we investigate the impact of reducing the number of snapshots on performance. The problem of short data snapshots for DoA algorithms has been extensively studied for linear arrays in the literature [12] and to a lesser extent for rectangular arrays [13], but in both cases, only isotropic radiators were considered. In [14], a linear array of independent isotropic radiators was studied with single snapshots and multiple snapshots. Mutual coupling (MC) effects were computed and taken into account in [15] and [16] for a linear array of dipoles, and also for spherical antenna arrays [17], [18], [19]. Instead, in this paper, we address MC through either measured or simulated ERPs, which intrinsically consider the platform and MC effects [20]. The approach incorporates and handles MC in a broader and more general sense if compared to [15], [16], [17], [18], and [19].

The paper is structured as follows; in Section II, we present the design of the single tag antenna, which is also used as the single element of the 3×3 array. Section III introduces the reference scenario and a simplified mathematical model of BLE DoA. Section IV presents a new approach to DoA estimation based on the use of Embedded Radiation Patterns (ERPs). Section V provides a brief overview of the MUSIC and Bartlett algorithms and discusses their computational complexity. Section VI presents extensive results for performance estimation under different conditions. The final Section provides a summary of the conclusions.

II. ANTENNA DESIGN

Both tag antenna and locator are probe-fed, monolithic, and circularly polarized patch antennas [21]. In particular, we consider a two-layer stack-up to accommodate 9 octagonal right-handed circularly polarized (RHCP) microstrip antennas along with the feeding network based on a grounded coplanar waveguide (GCPW) [22], [23]. The locator demonstrates a compact and flat configuration in comparison to other antenna array setups [17]. The two-layer stack-up incorporates a fence of cylindrical vias in the transition from the Grounded Co-Planar Waveguide (GCPW) to the probe and demonstrates advantages over existing literature [22, Tab. 2].

As shown in Fig. 1, a fence of circular vias has been implemented in the routing substrate between inner ground and slotted grounds to reduce long feed inductance, resulting in optimal antenna performance according to an extensive

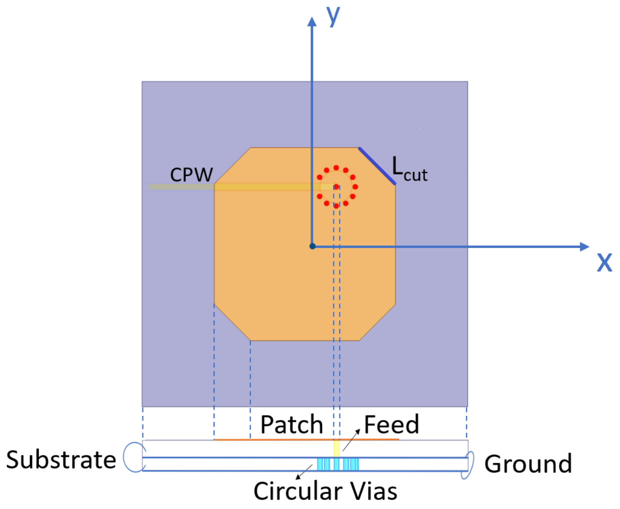

FIGURE 1. **Top and side views of designed tag. A two-layer stack-up fed by a GCPW is adopted. A fence of cylindrical vias is used to reduce long feed inductance instead of using capacitive compensation techniques [24]. Substrate dielectric constant with $\varepsilon_r = 4.8$ is adopted. The antenna, operating in the 2.4 GHz Bluetooth Low Energy band (BLE), is designed for Direction Finding (DF) applications.**

TABLE 1. **Antenna geometric parameters. The effective dielectric constant of the substrate is $\epsilon_{r,eff} = 4.8$.**

Parameter	Description	Value (mm)
L_x	Patch x-length	28.02
L_y	Patch y-length	29.88
f_x	Feeding point, x coordinate	4.83
f_y	Feeding point, y coordinate	8.85
h_1	Substrate 1 height	2.065
h_2	Substrate 2 height	1.565
$S_x = S_y$	Substrate and ground x,y-lengths	50
L_{cut}	Length of the cut (edge)	8.38

parametric study. A complete description of the geometric antenna parameters can be found in Tab. 1. Moreover, in Fig. 2 the final antenna impedance matching has been evaluated in the bandwidth (BW) [2, 2.8] GHz. As it is apparent, $|s_{11}| < -10$ dB has been obtained in the band [2.37, 2.53] GHz (corresponding to a 6.53% bandwidth).

In Fig. 3, a CP BW of 3.1% for a 6-dB threshold and a CP BW of 1.59% for a 3-dB threshold in Axial ratio (AR) has been achieved. A 6-dB AR gain can be considered satisfactory for the specific BLE application. Additionally, a co-polar gain of approximately 4 dB at 2.45 GHz has been achieved. These results have been experimentally validated. In the appendix, we present the pattern measurements and axial ratio (AR) for the 3 × 3 array locator employing the octagonal element.

Finally, we show a preliminary version of the proposed CP locator in Fig. 4. The locator is comprised of $M = 9$ CP patch antennas, as described previously. The full-wave simulations of the 3 × 3 arrays take into account MC and platform effects for various antenna spacing configurations. The octagonal shape enables final tuning even in the presence of drifts with respect to the nominal substrate dielectric constant, by acting

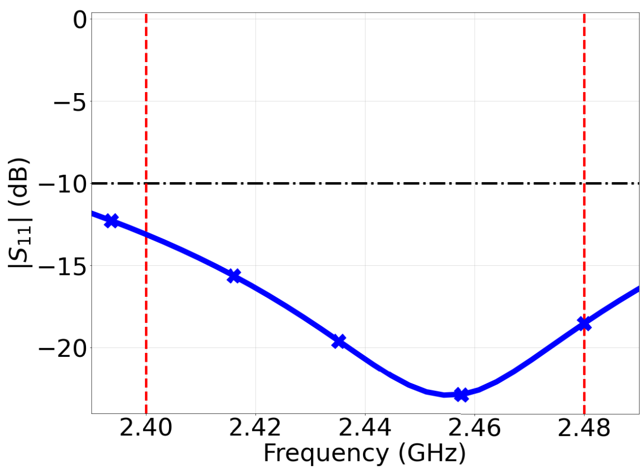

FIGURE 2. **Simulated $|s_{11}|$ for the designed tag antenna. An impendence BW of 6.53% has been achieved. For our applications, we are focused on the Bluetooth Low Energy (BLE) range ([2.4 – 2.48] GHz). It ensures good performance since it exceeds this range indicated by two dotted vertical lines.**

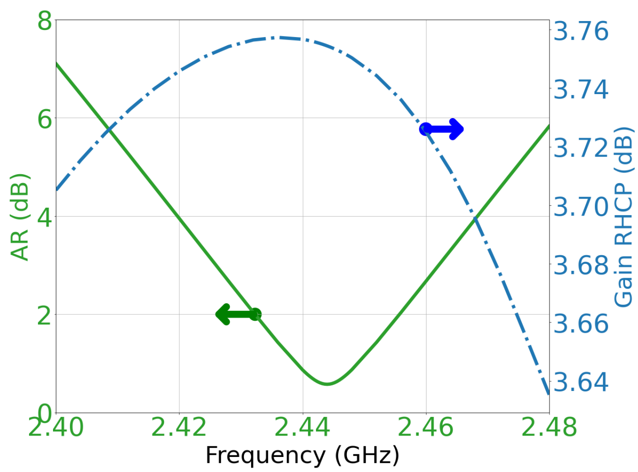

FIGURE 3. **Simulated AR and RHCP gain for the designed tag antenna. AR in the broadside direction ($\theta = 0$ and $\phi = 0$), the BW% = 3.1%. RHCP gain at 2.45 GHz frequency is 4 dB.**

on patch corners. The figure also shows the bottom-feeding network for the sake of clarity.

III. SYSTEM MODEL

DF is possible thanks to the introduction of the so-called Constant Tone Extension (CTE) in the end of the BLE packets, which consists of a sequence of alternating switch and sample slots, each either 1 μs or 2 μs long, as specified by the host [25].

The CTE has a variable length between 16 μs and 160 μs. During the IQ sampling process BLE receiver or locator extracts only CRC-valid packets. Considering the switch slot duration T_{switch} and the sampling slot duration T_{sample}, the locator controller extracts In-phase and Quadrature (IQ) samples during the CTE sample slots at the frequency $F_{\text{IQsamp}} = \frac{1}{T_{\text{switch}}+T_{\text{sample}}}$.

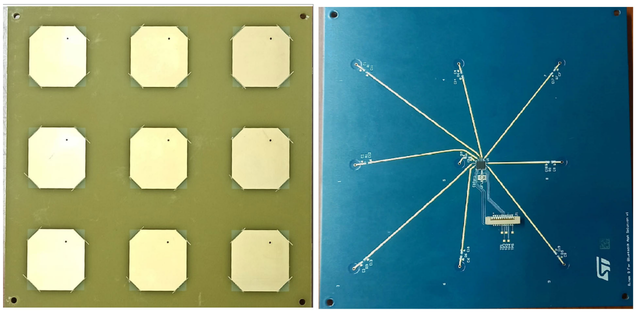

FIGURE 4. Top and bottom layer of the BLE locator composed of 9 elements arranged in a 3 × 3 URA9 array with an inter-element distance $d = 0.4\lambda = \frac{\lambda}{2.5} = 50$ mm. A switch operating in the BLE range is placed in the bottom layer to select each element. Strip lines with different lengths are used to connect the patches to the switch.

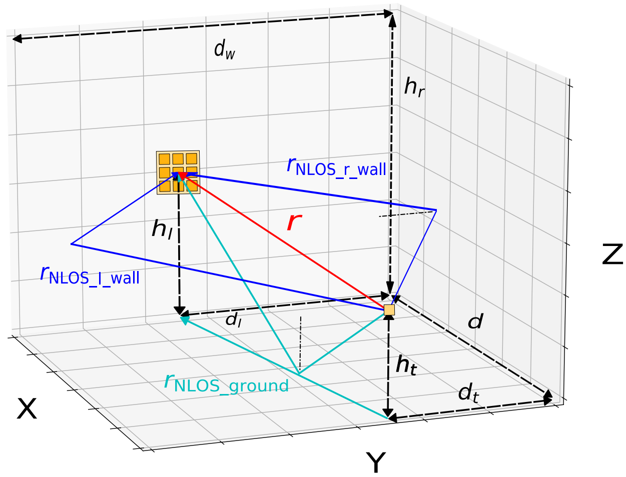

FIGURE 5. In our applications a two-ray model for an indoor environment is applied to tag and locator at heights h_t and h_l respectively from the floor. The line of Sight (LOS) path is shown by a solid red line. No LOS paths take into account the effect of reflection on the roof, floor, and side walls.

These IQ samples are arranged in a matrix, hereafter labeled by $[\underline{\mathbf{X}}]$. This matrix has M rows and N_{samp} columns, where M is the number of antennas and N_{samp} is the number of samples for each antenna. Each column is referred to as a "snapshot". The $[\underline{\mathbf{X}}]$ matrix is the input data for DoA algorithm. By setting the CTE time equal to 160 μs, we get less than $N_{\text{samp}} = 8$ samples per antenna or snapshot. Moreover, we consider only packets with valid CRC.

The mathematical model adopted to describe signal propagation only accounts for coherent reflections of the useful signal. This is because, in BLE 5.1, the non-coherent power of adjacent channels is negligible thanks to the receiver filtering chain. Therefore, all interfering signals arise from reflections (coherent interferences) of the useful signal itself.

Considering an indoor environment, there may be more than one reflection reaching the locator: generally, the dominant reflection is from the ground, then the one from the roof, then reflections from unintentional reflectors placed sideways to the path, and finally also reflections from obstacles behind the locator. To model such a propagation environment with an appropriate relative power P_i, a two-ray model is exploited for each reflection. The Line-of-Sight (LOS) distance tag-locator is r. The heights of the tag and locator with respect to the ground are h_t and h_l, and the ground-roof vertical distance is h_r. In the same way, we assume that the tag and locator are at the distances d_t and d_l from the right wall; similarly, the distance between lateral walls is d_w.

The typical propagation environment is depicted in Fig. 5. The LOS distance, r, between tag and locator can be calculated as:

$$r = \sqrt{d^2 + |h_t - h_l|^2 + |d_t - d_l|^2}\,. \tag{1}$$

The Non-Line-of-Sight (NLOS) wave paths reflected by the ground, roof and walls can be expressed as

$$\begin{aligned} r_{\text{NLOS\_ground}} &= \sqrt{r^2 + 4h_t h_l}\,, \\ r_{\text{NLOS\_roof}} &= \sqrt{r^2 + 4(h_r - h_t)(h_r - h_l)}\,, \\ r_{\text{NLOS\_r\_wall}} &= \sqrt{r^2 + 4d_t d_l}\,, \\ r_{\text{NLOS\_l\_wall}} &= \sqrt{r^2 + 4(d_w - d_t)(d_w - d_l)}. \end{aligned} \tag{2}$$

Equations (1)-(2) simply incorporate the Euclidean distance in the ray model depicted in Fig.5. For the sake of brevity, we introduce the following notation, which will be used throughout the paper:

$$r_{\text{NLOS},d} \in \{r_{\text{NLOS\_ground}}, r_{\text{NLOS\_roof}}, r_{\text{NLOS\_l\_wall}}, r_{\text{NLOS\_r\_wall}}\}\,. \tag{3}$$

Then, by using the two-ray model [26, Eq. (9,10)] and assuming the tag as a nearly isotropic radiator, the relation between the LOS path loss L_{LOS} of the direct signal and the NLOS path loss $L_{\text{NLOS,d}}$ due to the reflected signals is given by the Friis formula for radio-links in decibel:

$$L_{\text{NLOS,d}} = L_{\text{LOS}} + 10\log_{10}\left(\frac{r}{r_{\text{NLOS,d}}}\right)^2 + 10\log_{10}|\Gamma_{\text{refl}}|\,, \tag{4}$$

where $|\Gamma_{\text{refl}}|$ is the reflection coefficient by sidewalls, assuming it to be a random value varying within the interval $[0.2 - 0.6]$. Hence, the power of the signal arriving from the direction d can be expressed as:

$$P_d = \begin{cases} P_0 = P_t + L_{\text{LOS}}\,, & \text{for LOS signal} \\ P_{NLOS} = P_t + L_{\text{NLOS}}\,, & \text{for NLOS signals} \end{cases} \tag{5}$$

where P_t is the radiated power emitted by the tag.

More advanced models can incorporate not only material properties but also other factors, such as the incidence angle and polarization mismatch introduced by reflection, in this coefficient. For instance, we propose the use of CP to significantly reduce the coefficient. We simplify the model further by assuming that $h_t + h_l = h_r$ and $d_t + d_l = d_w$. Using these assumptions, we generate a typical statistical model for one incoming signal and its reflections.

The response of the rectangular antenna array to the $D+1$ impinging signals at a specific n-th snapshot is described by the array response matrix $[\underline{\mathbf{A}}] \in \mathbb{C}^{M\times(D+1)}$, that is:

$$[\underline{\mathbf{A}}] = [a(\phi_0,\theta_0),\cdots,a(\phi_i,\theta_i),\cdots,a(\phi_D,\theta_D)], \quad (6)$$

where the index $d \in \{\mathrm{LOS},\mathrm{NLOS}_1\ldots\mathrm{NLOS}_d\}$ scans the directions of arrival of the $D+1$ impinging signals, $a(\phi_d,\theta_d) \in \mathbb{C}^{M\times 1}$ are column vectors containing the $M = 9$ response of the array due to the signal arriving from the direction d sampled at the M ports of the array. The $[a]_d$ are known since can be measured or simulated for the various directions of arrival $d \leftrightarrow \underline{\Theta}_d = (\theta_d,\phi_d)$.

The base-band samples at the BLE receiver, running at a proper sample period T_s without ADC impairments can be expressed as:

$$[\underline{\mathbf{X}}_{\mathbf{ADC}}] = [\underline{\mathbf{A}}]\begin{bmatrix} E_0 & 0 & \cdots & 0 \\ 0 & E_1 e^{j\Delta_1} & 0 & 0 \\ \vdots & 0 & \ddots & \vdots \\ 0 & 0 & \cdots & E_d e^{j\Delta_D}\end{bmatrix}\begin{bmatrix} s_0 \\ s_1 \\ \vdots \\ s_D\end{bmatrix} + [\underline{\mathcal{N}}]\,. \quad (7)$$

In (7), the matrix $[\underline{\mathbf{E}}] = \mathrm{diag}(E_d e^{j\Delta_d})$, with $E_d \propto \sqrt{P_d}$, considers the relative amplitudes of the $D+1$ impinging signals; Δ_d is the phase shift coefficient due to reflected paths, including the reflection coefficient phase $\angle\Gamma$. $[\underline{\mathbf{s}}]$ is a signal matrix of dimension $(D+1)\times N_{\mathrm{samp}}$ formed by $D+1$ row vectors, $(s_0, s_1,\cdots,s_{D+1}) = (s_0,s_0,\cdots,s_0)$, each of dimension $1\times N_{\mathrm{samp}}$; similarly $[\underline{\mathcal{N}}] = [n_0\ n_1\ \cdots\ n_m]^T$, a $M\times N_{\mathrm{samp}}$ matrix, is the additive white Gaussian noise (AWGN) with zero mean and variance σ^2 added at the M antenna ports. The matrix $[\underline{\mathbf{X}}_{\mathbf{ADC}}]$ of $M\times N_{\mathrm{samp}}$ as previously defined in (7), needs to be low-pass filtered and down-sampled to the F_{IQsample}, obtaining $[\underline{\mathbf{X}}]$, an $M\times N_{\mathrm{snap}}$. The signals $s_d(i)$ are 2GFSK base-band signals at the Analog-to-Digital Converter (ADC) of the Bluetooth receiver:

$$s_d(i) = \mathrm{e}^{\mathrm{j}\alpha(i)}\,, \quad (8)$$

where $\alpha(i) = \alpha_0 + \frac{h\pi}{I_s}\sum_{k=0}^{i} b_d p(k - iI_s)$, i represents the discrete-time index, I_s is the integer number of samples per symbol period, h is the modulation index, $p(i)$ is the symbol pulse, and $b_d \in \{1,-1\}$ are the binary symbols to be transmitted. In the mathematical model of the baseband CTE, it is sufficient to set the binary symbols b_d equal to 1 in (8).

IV. CSV AND ERP TECHNIQUES FOR THE DOA ESTIMATION

For DoA estimation, the nine-element array is described by its array response, which is computed for all possible incoming angles.

The conventional steering vector (CSV) approach considers only the phase shifts measured at each port of the single element of the array. In practice, the signal amplitudes and phases are collected in a complex array, denoted by $[A_0, A_1,\cdots,A_8]$. However, since the elements are isotropic, only the phases, denoted by $\Psi_m = \angle A_m$, at each antenna port are considered.

The theoretical CSV array pattern for all possible directions can be defined as:

$$a(m,\phi,\theta) = \mathrm{e}^{\mathrm{j}\frac{2\pi}{\lambda}\sin\theta[p_x(m)d_x\cos\phi + p_y(m)d_y\sin\phi]}\,, \quad (9)$$

where the index $m \in [0,8]$ scans the 9 elements of the URA9 array, with $p_x = [0,1,2,0,1,2,0,1,2]$, $p_y = [0,0,0,1,1,1,2,2,2]$ the positions of the patch m along x and y measured in units of d [27].

For computation purposes, the array response can be sampled for different "discrete" directions of arrival with a running index l; the discrete directions are then $\underline{\Theta}_l = (\theta_l,\phi_l)$ and the CSV can be stored in a matrix, namely

$$S(:,\phi_l,\theta_l) = [s_{m,l}] = [\underline{\mathbf{S}}] = [\mathrm{e}^{\mathrm{j}\Psi_0},\mathrm{e}^{\mathrm{j}\Psi_1}\cdots\mathrm{e}^{\mathrm{j}\Psi_{L-1}}]\,, \quad (10)$$

which is the sampled version of (9). The matrix $[\underline{\mathbf{S}}]$ has dimensions $M\times L$, where $l \in \{0,1,\cdots L-1\}$ scans the possible directions of arrival. L is the product JK, being J the number of angles θ_j, taken along the θ angle (here $\theta = 90 - \vartheta_{\mathrm{Elevation}}$), and K, the number of angles ϕ_k, taken along the azimuth angle ϕ. If we scan with a step of one degree in the polar system we have $\theta_j \in [0°, 1°,\ldots 180°]$, $J = 181$, and $\phi_k \in [0°, 1°,\ldots 359°]$, $K = 360$ thus $L = JK = 65160$. In some approaches, it can be useful to represent the L directions of arrival in terms of directional cosines, in place of (θ_l,ϕ_l).

The CSV analytical approach is based on the geometrical arrangement of ideal isotropic radiators, but it has limitations. Specifically, this approach does not consider pattern elements and does not consider mutual coupling between elements.

The novel approach proposed here leverages measured or simulated effective radiated patterns (ERPs) and takes into account both mutual coupling and mounting-platform effects [20]. The ERP is used to evaluate the "steering vectors" $[\underline{\mathbf{S}}]$, that are no more calculated by (10). Embedded radiation patterns in our case are calculated by full-wave simulations, that evaluate the field radiated by each antenna of the array (with the other antennas terminated on a matched load). Also for ERP, we export data from full-wave simulation by adopting the scanning intervals $\theta \in [0:180]$ and $\phi \in [0:359]$ respectively, in the standard spherical coordinate system. It is thus possible to evaluate not only the phase of the incoming signal, measured at the antenna port but also its amplitude, which strongly depends on the single-element gain pattern. The received amplitudes and phases are exported in a table for each element array. The ERP array response $[s_{m,l}]$ can be defined as:

$$a(m,\phi,\theta) = a_{\mathrm{ERP}}(m,\phi,\theta), \quad (11)$$

where a_{ERP} represents either the output of a full wave simulation or the result of an accurate experimental characterization.

The ERP approach leverages the full-wave characterization of the antenna array. This enhancement can also be applied in a compact array version, with closely spaced elements, where the oversimplified CSV approach falls short.

V. MUSIC AND BARTLETT ALGORITHMS

The BLE receiver filtering chain allows us to consider only coherent impinging signals. In the model described in the previous section, we considered only coherent replicas of the incoming signal impinging from different directions.

In this section, despite the well-known fact that MUSIC does not perform well with coherent signals, we still use it alongside the standard beamformer Bartlett, as MUSIC represents a reference model. The MUSIC and Bartlett algorithms are detailed in Algorithm 1 and in Algorithm 2, respectively.

Algorithm 1 MUSIC

function MUSIC (X, S);
Input : The complex matrix $[\underline{\mathbf{X}}]$ of IQ samples and the complex $M \times L$ matrix of embedded radiation pattern $[\underline{\mathbf{S}}]$
Output: *pseudospectrum*
$R \leftarrow E\left\{XX^H\right\}$
$[Q, eig, V] \leftarrow SVD(R)$
$Q_n \leftarrow Q(:, M : N)$
$pseudospectrum \leftarrow \frac{S^H S}{S^H Q_n Q_n^H S}$
return *pseudospectrum*

Algorithm 2 Bartlett

function Bartlett (X, S);
Input : The complex matrix $[\underline{\mathbf{X}}]$ of IQ samples and the complex $M \times L$ matrix of embedded radiation pattern $[\underline{\mathbf{S}}]$
Output: *pseudospectrum*
$R \leftarrow E\left\{XX^H\right\}$
$pseudospectrum \leftarrow \frac{S^H R\, S}{S^H S}$
return *pseudospectrum*

Both MUSIC and Bartlett share the first step, which is the evaluation of the covariance matrix $\underline{\mathbf{R}} = \mathbf{E}\left\{\underline{\mathbf{XX^H}}\right\}$.

In the MUSIC algorithm, the eigenvectors of the noise subspace, $\underline{\mathbf{Q}}_{\mathbf{n}}$, are obtained from the covariance matrix $\underline{\mathbf{R}}$, and are subsequently used to calculate the pseudo-spectrum:

$$P_{\text{MUSIC}}(\Theta) = \frac{\underline{\mathbf{S}}(:, \Theta)^H \underline{\mathbf{S}}(:, \Theta)}{\underline{\mathbf{S}}(:, \Theta)^H \cdot \underline{\mathbf{Q}_\mathbf{n}} \cdot \underline{\mathbf{Q}_\mathbf{n}}^H \cdot \underline{\mathbf{S}}(:, \Theta)}. \tag{12}$$

In equation (12), $[\underline{\mathbf{S}}]$ denotes the radiation pattern matrix, which is either calculated using the CSV approach or obtained from measurement/simulation using the ERP method.

In the Bartlett method, the pseudo-spectrum is obtained directly from the covariance matrix $\underline{\mathbf{R}}$, without the need for calculating the singular value decomposition (SVD).

$$P_{\text{Bartlett}}(\Theta) = \frac{\underline{\mathbf{S}}(:, \Theta)^H \underline{\mathbf{R}} \cdot \underline{\mathbf{S}}(:, \Theta)}{\underline{\mathbf{S}}(:, \Theta)^H \cdot \underline{\mathbf{S}}(:, \Theta)}. \tag{13}$$

In (12) and (13) we used $\underline{\Theta}_l = (\theta_l, \phi_l)$ and the "weighted" formulas as described in [28].

A. ALGORITHM COMPLEXITY

Figure 6 illustrates the one-to-one relationship, $[s_{m,l}] = a(m, \phi_l, \theta_l)$, between incoming signals and retrieved phases. However, to determine the direction of arrival, this relationship needs to be inverted.

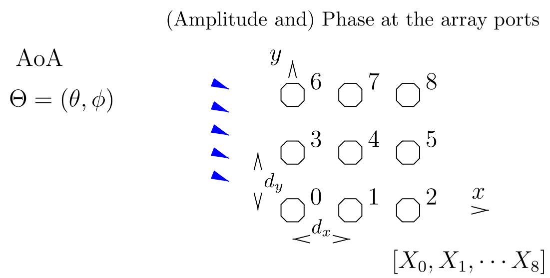

FIGURE 6. Biunivocal (one-to-one) relationship between the incoming signal direction, Θ, and the corresponding vectors $[\underline{\mathbf{S}}] = [\mathbf{S_0}, \mathbf{S_1}, \cdots, \mathbf{S_8}]$ called "data-sets". By inverting this relation is possible to determine the DoA.

The complexity of each algorithm depends on the number of antennas and on the number of snapshots. Given the "large size" of $[\underline{\mathbf{S}}]$, it is evident that the computational complexity mainly depends on the calculation of the pseudo-spectrum. However, if the number of snapshots required to achieve specific detection performances is very high, the collection time of the various snapshots becomes predominant over the algorithm computation time.

VI. MUSIC AND BARTLETT PERFORMANCE ESTIMATION

The effectiveness of the mathematical model presented in the previous section is tested here for different locator sizes, signal configurations, and noise conditions. Extensive numerical analysis has been carried out by considering realistic 3D embedded patterns from specific designs considered here (see Fig. 4). The performance of MUSIC and Bartlett algorithms have been tested by considering only the incident signal (LOS) or both the incident signal and two NLOS interfering signals, by varying the signal-to-noise ratio (SNR) of the system.

A. LOCATOR SIZE

As a first step, we conducted a performance analysis to find a balance between antenna miniaturization and accuracy.

Throughout the analysis, we generated and stored a statistical model for the incoming signals, which allowed us comparing the performance of different layouts. The angles of arrival considered are $\theta \in [0°, 85°]$ and $\phi \in [0°, 360°]$. The SNR is referred to the ADC frequency, F_{ADC}, and to the received power of the LOS path, P_0. Cases with 80, 8, and 1 snapshots have been simulated, where 8 snapshots correspond to 1 packet. For these tests, the distance between the locator and the tag, d, has been chosen randomly in a range between 1 and 9 meters. The selected distance between the roof and the floor, h_r, has been taken equal to 4 meters while the distance between the walls, d_w, has been randomly chosen up to 6 meters. Moreover, the reflection coefficient of the materials, Γ_{refl}, has been chosen randomly in the interval [0.2, 0.6].

The effectiveness of various antenna layouts through extensive numerical analysis is now considered. It is worth mentioning that all comparisons have been made by assuming the same incoming signal statistics, thus under equal conditions. To obtain a better configuration in terms of tracking accuracy and miniaturization, three array structures have been taken into account, respectively with an inter-element distance $\frac{d}{\lambda} = [0.5, 0.4, 0.35]$.

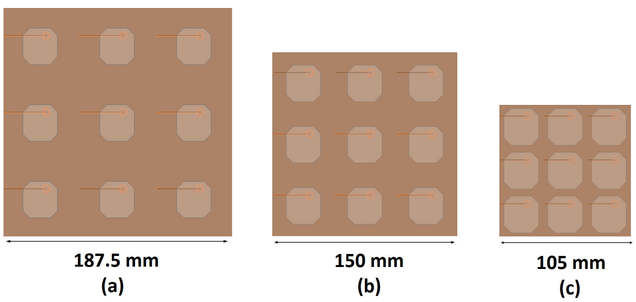

FIGURE 7. 3 × 3 array configuration with different inter-element distances: (a) $d = \frac{\lambda}{2.0}$, (b) $d = \frac{\lambda}{2.5}$, (c) $d = \frac{\lambda}{3.5}$. We aim to assess a trade-off between tracking accuracy and miniaturization. By reducing the size of the array, a substantial decrease in gain is observed. More precisely, the gain value for an individual radiator decreases from 3.4 dB to 0.5 when the spacing between the elements changes from (a) to (c).

As shown in Fig. 7, a reduction in size of 20% and 30% is achieved by moving from (a) to (c). However, this size reduction also results in a significant decrease in gain. Specifically, the gain drops from 3.4 dB for a single radiator at 2.44 GHz in the 3 × 3 array with a $d = \frac{\lambda}{2.0}$ spacing, to 2 dB for a $d = \frac{\lambda}{2.5}$ spacing, and 0.5 dB for a $d = \frac{\lambda}{3.5}$ spacing.

The performance analysis was conducted to evaluate the impact of locator size on DoA estimation accuracy. The ERP approach was used to account for mutual coupling effects and gain loss due to miniaturization.

The Mean Absolute Error (MAE) served as the performance metric to assess the accuracy of the main direction of arrival detection. MAE represents the average absolute error between the true angle of arrival (ground truth), ψ, and its estimation, $\hat{\psi}$, averaged over N measurements. MAE can be

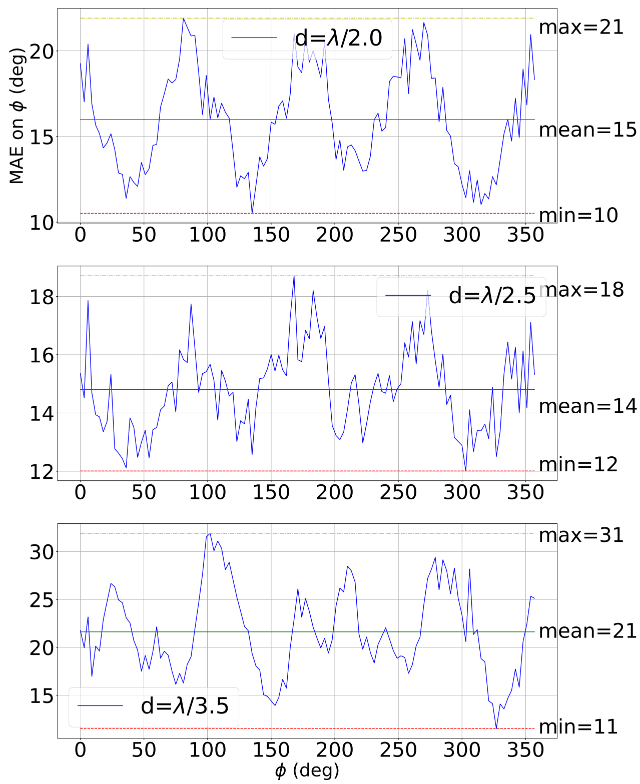

FIGURE 8. Impact of inter-element distance d with 2 NLOS and ERP approach. MAE using MUSIC algorithm, 1 degree resolution on azimuth ϕ. The MAE analysis reveals more accurate estimates (minimum, mean, maximum) across the azimuthal range ϕ when the $d = \frac{\lambda}{2.5}$ spacing is employed.

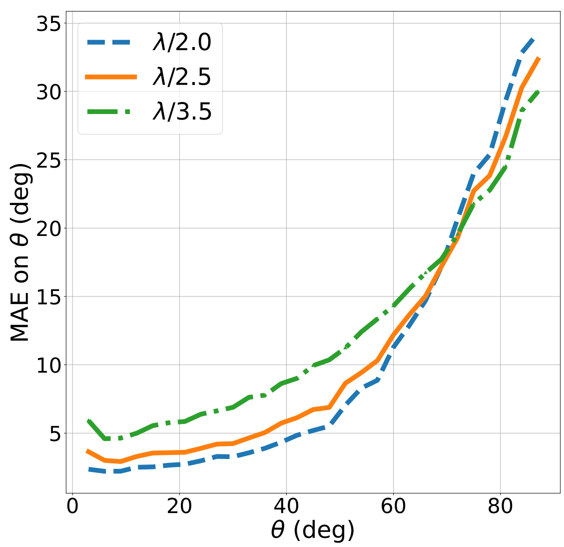

FIGURE 9. Impact of inter-element distance d with 2 NLOS and ERP approach. MAE using MUSIC algorithm, 1-degree resolution on θ. In this case, the MAE value increases for grazing angles since the gain becomes negligible at these angles. For $\theta < 70°$, $d = \lambda/2$ spacing demonstrates superior performance, while for $\theta > 70°$, $d = \lambda/2.5$ spacing is the recommended compromise. As a result of the MAE analysis over θ and ϕ, the spacing $d = \frac{\lambda}{2.5}$ configuration is chosen for the locator design.

calculated individually for the elevation, $\psi = \theta$, and for the azimuth, $\psi = \phi$. The definition of MAE over θ is the following [29, (42)]:

$$\mathrm{MAE}_\theta = \sum_n \frac{|\theta_n - \hat{\theta}_n|}{N} \tag{14}$$

The MAE over ϕ has been estimated by exploiting the concept of cosine directors; namely, true and estimated directions along the azimuthal plane are associated to their unit vectors $\underline{\mathbf{u}}$ and $\hat{\underline{\mathbf{u}}}$.

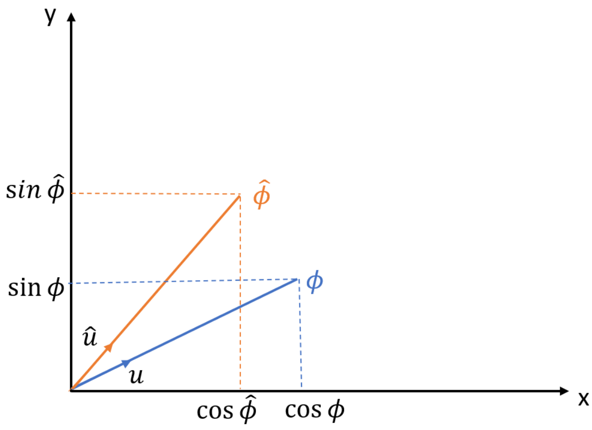

FIGURE 10. **MAE estimation in the ϕ plane. By adopting the cosine director approach the geometric angle between the two unit vectors u and $\hat{u}$ is calculated.**

$$\underline{\mathbf{u}} = \cos\phi\,\hat{\mathbf{u}}_x + \sin\phi\,\hat{\mathbf{u}}_y$$
$$\hat{\underline{\mathbf{u}}} = \cos\hat{\phi}\,\hat{\mathbf{u}}_x + \sin\hat{\phi}\,\hat{\mathbf{u}}_y \tag{15}$$
$$\mathrm{MAE}_\phi = \sum_n \frac{\arccos(\cos\phi_n\cos\hat{\phi}_n + \sin\phi_n\sin\hat{\phi}_n)}{N}$$
$$= \sum_n \frac{\arccos[\cos(\hat{\phi}_n - \phi_n)]}{N} \tag{16}$$

where N is the number of trials. The definition presented in equation (16) is equivalent to [29, (43)], with the notable difference that it effectively incorporates the periodicity of ϕ every 2π radians or 360 degrees.

Results for the error in the azimuth (ϕ) plane are presented in Fig. 8. The analysis reveals that the $\frac{\lambda}{2.5}$ configuration yields the highest accuracy based on the minimum, mean, and maximum MAE values.

In addition, as illustrated in Fig 9 for incidence at grazing, a large increase of MAE on θ is observed due to the negligible gain of patch antennas at such angles. As a result, the $\frac{\lambda}{2.5}$ array spacing was selected as optimal configuration, as it provides a good balance between the size of the array and DoA accuracy. This configuration is illustrated in Fig. 7(b) and will be used throughout the rest of the paper.

B. CSV VS ERP

It is useful to compare the performance of the MUSIC and Bartlett algorithms when using the CSV and ERP approaches. This provides insight on the impact of mutual coupling and gain loss on DoA estimation accuracy.

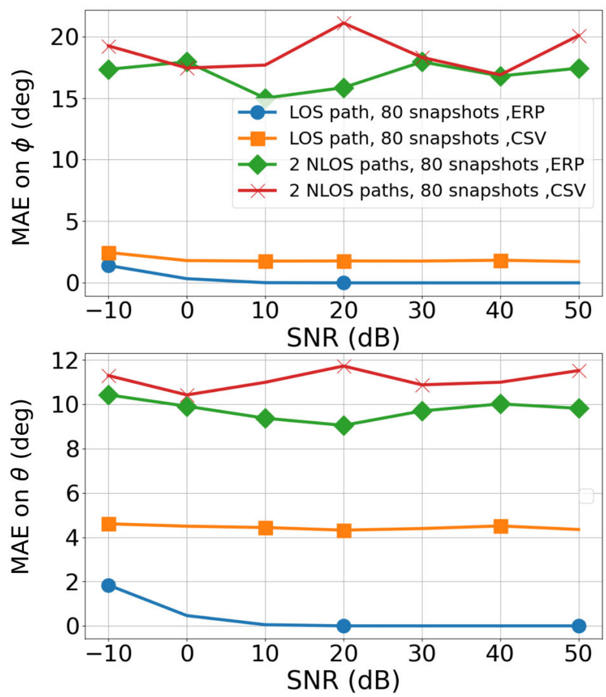

FIGURE 11. **ERP vs CSV approach comparison with 0 NLOS and 2 NLOS. MAE evaluation using MUSIC algorithm, 1 degree resolution on azimuth and elevation, 80 snapshots and inter-elements distance of $d = \frac{\lambda}{2.5}$ (Fig. 7(b)). ERP can compensate for frequency mismatching and mutual coupling between elements ensuring better performances in terms of SRN over θ and ϕ. Nonetheless, when multiple reflections are considered (i.e., NLOS paths), similar performances between ERP approach and CSV are achieved.**

Thanks to characterization, the ERP approach considers and "compensates" for mutual coupling between array elements. On the other hand, CSV is an analytical approach that requires less information on the array since does not account for these factors. As shown in Fig. 11, in a line-of-sight (LOS) environment, the ERP estimation over ϕ and θ is more accurate than CSV. In the presence of multipath, the performance with ERP is still higher than CSV as long as the number of non-line-of-sight (NLOS) paths does not degrade the signal-to-noise ratio (SNR). However, in a noisy scenario, the two approaches do not differ much.

In Fig. 12, an ERP comparison has been conducted considering 3×3 and 4×4 array configurations, for 0 NLOS and 2 NLOS paths. The evaluation of MAE on the azimuthal and elevation plane indicates that the 4×4 configuration outperforms the 3×3 configuration thanks to the higher spatial resolution of the larger array.

C. NUMBER OF SNAPSHOTS

We now evaluate system performances as the number of snapshots varies. We use the ERP in the analysis presented below.

In Fig. 13, the performance of the system is evaluated as the number of snapshots varies. It is observed that as the number of snapshots decreases, the Mean Absolute Error

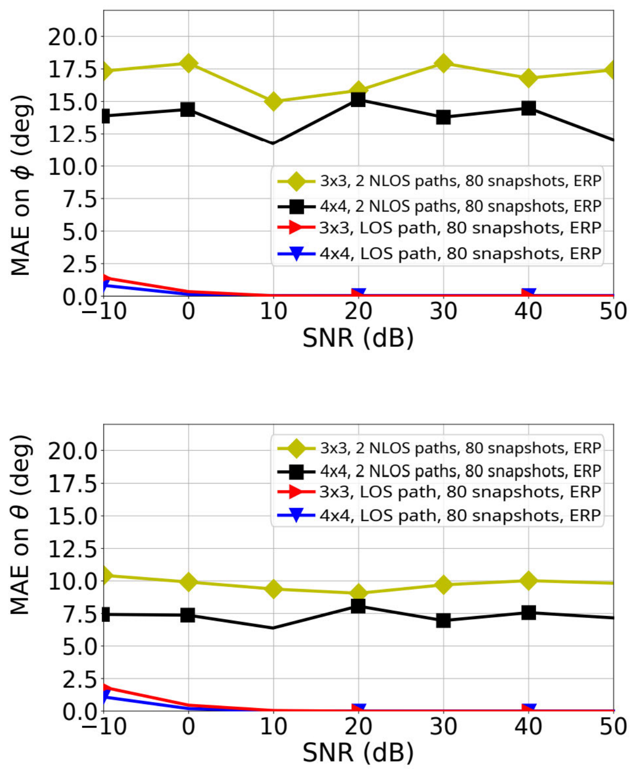

FIGURE 12. ERP approach comparison for 3 × 3 and 4 × 4 array configuration with 0 NLOS and 2 NLOS. MAE evaluation using MUSIC algorithm, 1 degree resolution on azimuth and elevation, 80 snapshots and inter-elements distance of $d = \frac{\lambda}{2.5}$ (Fig. 7(b)). 4 × 4 array configuration outperforms 3 × 3 on azimuth and elevation.

(MAE) increases, indicating a decrease in performance. The degradation is noticeable when the number of snapshots is reduced from 80 to 8, especially for signal-to-noise ratios (SNR) below 0 dB. The degradation is even more significant for a single snapshot, especially for signal-to-noise ratios (SNR) less than 10 dB. Neither of the two presented algorithms outperforms the other in the case under test. This observation is consistent with the fact that MUSIC does not provide any advantage over conventional beamformers in the presence of coherent signals.

In the case of two reflections, as shown in Fig. 14, the MAE gets worse in the case of azimuthal acquisition: about 15 degrees at SNR = 20 dB. Instead, about 9 degree degradation is observed in elevation. In particular, when SNR > 20 dB very similar performances are achieved as the number of snapshots varies. This implies that for high SNRs the accuracy resolution does not depend on the number of snapshots, with a significant reduction on the overall computational burden if only one snapshot is used. Again, MUSIC and Bartlett exhibit similar performances.

For 4 NLOS, both the ERP and CSV approaches were found to fail, due to large number of coherent interferences, which degraded the SNR. However, we do not report the results for 4 NLOS, since the use of CP effectively limits the number of coherent reflections. Moreover, the scenario with 4 strong NLOS signals is not very common in real scenarios, when both tag and locator use CP.

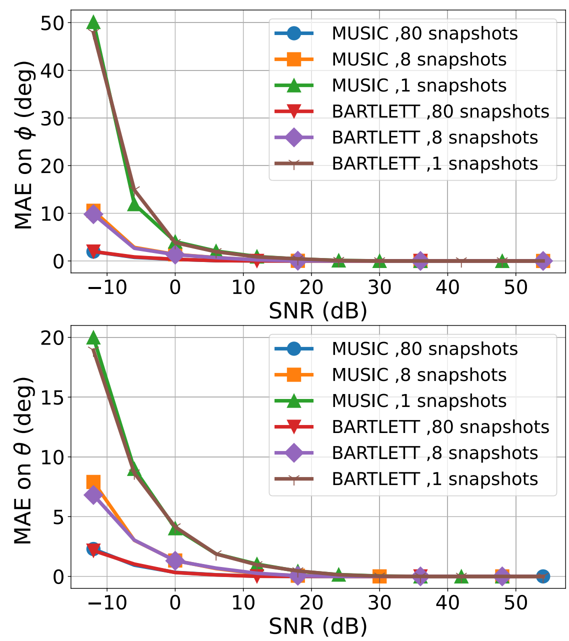

FIGURE 13. Comparison between MUSIC and Bartlett algorithms by varying the number of snapshots with 0 NLOS. MAE evaluation, 1 degree resolution on azimuth and elevation. When the number of snapshots decreases the performance in terms of MAE deteriorates. Specifically, a noticeable degradation is observed for SNR less than 0 dB when reducing the snapshots from 80 to 8. Considering only 1 snapshot results in a performance deterioration, especially for SNR values less than 10 dB.

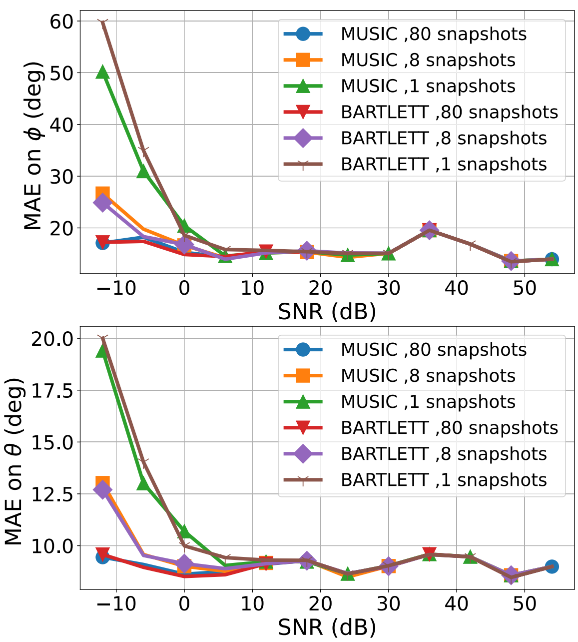

FIGURE 14. Comparison between MUSIC and Bartlett algorithm by varying the number of snapshots with 2 NLOS. MAE evaluation, 1 degree resolution on azimuth and elevation. As shown, for high SNR (i.e.>20 dB), the accuracy does not depend on the number of snapshots, thus allowing faster computation.

VII. COMPLEXITY ORDER OF SUBSPACE-BASED AND COMPRESSIVE SENSING METHODS

Subspace-based algorithms like MUSIC or ESPRIT derive two orthogonal subspaces performing the eigen-decomposition of the covariance matrix of the received signals for the computation of the DoA. It implies a high computational complexity, since snapshots are needed for data-sampled covariance matrix calculations. Despite the subspace-based algorithm's low complexity new methods for DoA based on the spatial sparsity of the spectrum as OMP or the Focused Orthogonal Matching Pursuit (FOMP) have been introduced [2], [4]. Similarly, 3D-OMPS and 3D-FOMP [7] perform a lower computational complexity with respect to the 3D-MUSIC and 3D-ESPRIT [1], [9]. Also, HOMP shows a lower computational complexity with respect OMP or FOMP when the number of array elements is greater than 2 [6].

TABLE 2. Complexity order of the main DoA algorithms depending on the number of array radiators (N), the number of incoming sources (M), the number of snapshots (K), the discrete grid of DoAs (P), the size of different dictionaries H AND H'.

Schemes	Complexity
MUSIC [1]	$\mathcal{O}(N^2P + N^2K)$
ESPRIT [9]	$\mathcal{O}(N^3 + N^2K)$
OMP [2]	$\mathcal{O}(2HNK) + \mathcal{O}(HM)$
FOMP [4]	$\mathcal{O}(H^2NK) + \max(\mathcal{O}(HM), \mathcal{O}(2H'^2M))$
HOMP [6]	$\mathcal{O}(2H(N+1)K) + \mathcal{O}((H+H')M)$
3D-MUSIC [1]	$\mathcal{O}(N^4P + N^4K)$
3D-ESPRIT [9]	$\mathcal{O}(N^6 + N^4K)$
3D-OMP [7]	$\mathcal{O}(H^2N^2K) + \mathcal{O}(H^2M)$
3D-FOMP [7]	$\mathcal{O}(H^2N^2K) + \max(\mathcal{O}(H^2M), \mathcal{O}(H'^4M))$

Table 2 summarizes the results of the above-mentioned methods.

VIII. CONCLUSION

In this paper, the performance of a DoA locator-based BLE 5.1 has been evaluated by using a ray-based model. An approach based on embedded radiation patterns has been also introduced for two direction-finding algorithms, MUSIC and Bartlett.

The designed single antenna shows a simulated CP BW of 3.1% and 1.59% for a 6-dB and 3-dB threshold, respectively. A 6-dB AR gain can be considered satisfactory for the specific BLE application. Different realistic array configurations have been tested to achieve a trade-off between array dimension and DoA accuracy; the $d = \frac{\lambda}{2.5}$ inter-element array configuration best satisfies these requirements.

The performances, in terms of MAE, have been measured versus the number of IQ sample snapshots collected by the locator. The MAE was measured for different numbers of IQ sample snapshots collected by the locator, and it was observed that reduction of the number of snapshots leads to a predictable loss of signal-to-noise ratio (SNR). For the real non-isotropic array studied, the ERP guarantees better performances with respect to the CSV, both in LOS and NLOS environments. The results demonstrate that the ERP approach provides better performance than the CSV approach until the number of interferences degrades the SNR. For scenarios with sufficient signal-to-noise ratio, utilizing the measurements collected in a single snapshot can lead to a significant reduction in the overall computational load.

APPENDIX

In the manuscript, the ERP pattern is extensively employed; in this appendix, we demonstrate a reasonably strong agreement between the measured embedded radiation pattern and the simulated ones.

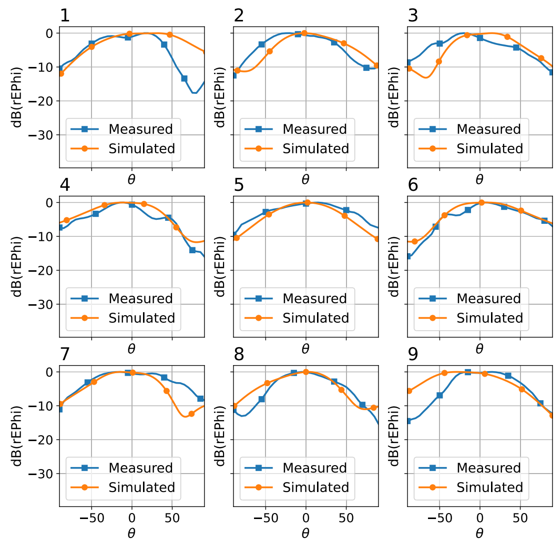

FIGURE 15. Comparison of the measured and simulated magnitudes of the ϕ component of the electric field, denoted as $|E_\phi|$, in the ϕ = 0-cut.

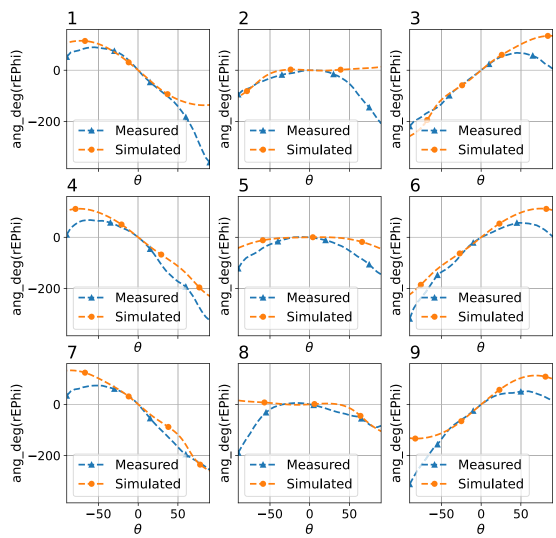

FIGURE 16. Comparison of the measured and simulated phases of the ϕ component of the electric field, referred to as $\angle E_\phi$, in the ϕ = 0-cut. In the figure, for the sake of clarity, we employ a shared reference phase of zero at θ = 0 for all patches, as each patch is connected through a path of varying length (see Fig. 4).

Multiple cuts and measurements have been performed, and we present one example here, where a pattern was obtained using a vertically polarized transmitting horn antenna, thereby selecting the E_ϕ polarization in the $\phi = 0$-cut (see Fig. 15 for magnitude and Fig. 16 for phase). Similar results were obtained in other polarizations/cuts.

The final verification, shown in Fig. 17, concerned the measured AR that was compared to the expected one.

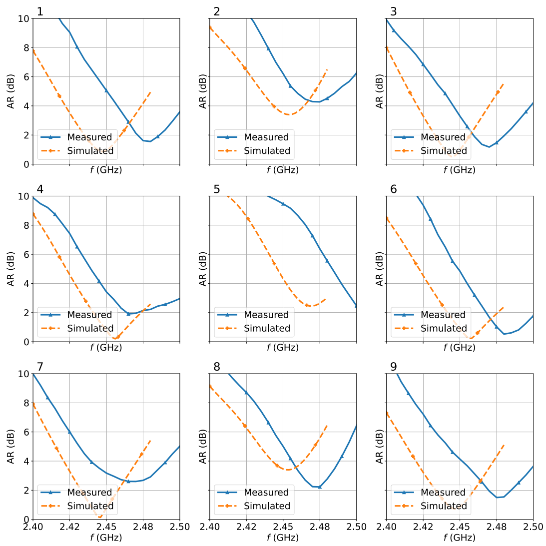

FIGURE 17. AR comparison between measurements and simulations for each patch. Measurement shows that AR is shifted respect simulations with central frequency around 2.48 GHz instead of 2.44 GHz of the simulations.

REFERENCES

[1] R. Schmidt, "Multiple emitter location and signal parameter estimation," *IEEE Trans. Antennas Propag.*, vol. AP-34, no. 3, pp. 276–280, Mar. 1986.

[2] S. K. Sahoo and A. Makur, "Signal recovery from random measurements via extended orthogonal matching pursuit," *IEEE Trans. Signal Process.*, vol. 63, no. 10, pp. 2572–2581, May 2015.

[3] A. Aich and P. Palanisamy, "On-grid DOA estimation method using orthogonal matching pursuit," in *Proc. Int. Conf. Signal Process. Commun. (ICSPC)*, Jul. 2017, pp. 483–487.

[4] M. Dehghani and K. Aghababaiyan, "FOMP algorithm for direction of arrival estimation," *Phys. Commun.*, vol. 26, pp. 170–174, Feb. 2018.

[5] Y. I. Abramovich and N. K. Spencer, "Design of nonuniform linear antenna array geometry and signal processing algorithm for DOA estimation of Gaussian sources," *Digit. Signal Process.*, vol. 10, no. 4, pp. 340–354, Oct. 2000.

[6] K. Aghababaiyan, V. Shah-Mansouri, and B. Maham, "High-precision OMP-based direction of arrival estimation scheme for hybrid non-uniform array," *IEEE Commun. Lett.*, vol. 24, no. 2, pp. 354–357, Feb. 2020.

[7] K. Aghababaiyan, R. G. Zefreh, and V. Shah-Mansouri, "3D-OMP and 3D-FOMP algorithms for DOA estimation," *Phys. Commun.*, vol. 31, pp. 87–95, Dec. 2018.

[8] C. Stoeckle, J. Munir, A. Mezghani, and J. A. Nossek, "DoA estimation performance and computational complexity of subspace- and compressed sensing-based methods," in *Proc. 19th Int. ITG Workshop Smart Antennas (WSA)*, Mar. 2015, pp. 1–6.

[9] R. Roy and T. Kailath, "ESPRIT-estimation of signal parameters via rotational invariance techniques," *IEEE Trans. Acoust. Speech Signal Process*, vol. 37, no. 7, pp. 984–995, Jul. 1989.

[10] S. C. Pavone, G. S. Mauro, L. D. Donato, and G. Sorbello, "Design of dual circularly polarized sequentially-fed patch antennas for satellite applications," *Appl. Sci.*, vol. 10, no. 6, p. 2107, Mar. 2020.

[11] H. Govindarajan, S. C. Pavone, L. D. Donato, P. D. Mariano, G. Distefano, P. Livreri, P. Nagaradjane, C. Squadrito, and G. Sorbello, "Design of a compact dual circular-polarized antenna for L-band satellite applications," *IEEE Antennas Wireless Propag. Lett.*, vol. 19, pp. 547–551, 2020.

[12] Q. S. Ren and A. J. Willis, "Extending MUSIC to single snapshot and on line direction finding applications," in *Proc. Radar Conf.*, Oct. 1997, pp. 783–787.

[13] M. Perrone, D. P. Pau, and N. I. Piazzese, "Constrained neural estimation of Bluetooth direction of arrival with non-uniform arrays," in *Proc. IEEE Int. Conf. Consum. Electron. (ICCE)*, Jan. 2022, pp. 1–6.

[14] M. Carlin, P. Rocca, G. Oliveri, F. Viani, and A. Massa, "Directions-of-arrival estimation through Bayesian compressive sensing strategies," *IEEE Trans. Antennas Propag.*, vol. 61, no. 7, pp. 3828–3838, Jul. 2013.

[15] P. Rocca, M. A. Hannan, M. Salucci, and A. Massa, "Single-snapshot DoA estimation in array antennas with mutual coupling through a multiscaling BCS strategy," *IEEE Trans. Antennas Propag.*, vol. 65, no. 6, pp. 3203–3213, Jun. 2017.

[16] O. J. Famoriji and T. Shongwe, "Electromagnetic machine learning for estimation and mitigation of mutual coupling in strongly coupled arrays," *ICT Exp.*, vol. 9, no. 1, pp. 8–15, Feb. 2023.

[17] O. J. Famoriji, O. Y. Ogundepo, and X. Qi, "An intelligent deep learning-based direction-of-arrival estimation scheme using spherical antenna array with unknown mutual coupling," *IEEE Access*, vol. 8, pp. 179259–179271, 2020.

[18] O. J. Famoriji and T. Shongwe, "Source localization of EM waves in the near-field of spherical antenna array in the presence of unknown mutual coupling," *Wireless Commun. Mobile Comput.*, vol. 2021, pp. 1–14, Dec. 2021.

[19] O. J. Famoriji and T. Shongwe, "Spherical atomic norm-inspired approach for direction-of-arrival estimation of EM waves impinging on spherical antenna array with undefined mutual coupling," *Appl. Sci.*, vol. 13, no. 5, p. 3067, Feb. 2023.

[20] A. F. Morabito, A. Di Carlo, L. Di Donato, T. Isernia, and G. Sorbello, "Extending spectral factorization to array pattern synthesis including sparseness, mutual coupling, and mounting-platform effects," *IEEE Trans. Antennas Propag.*, vol. 67, no. 7, pp. 4548–4559, Jul. 2019.

[21] O. Leonardi, M. G. Pavone, G. Sorbello, A. F. Morabito, and T. Isernia, "Compact single-layer circularly polarized antenna for short-range communication systems," *Microw. Opt. Technol. Lett.*, vol. 56, no. 8, pp. 1843–1846, Aug. 2014.

[22] O. Crisafulli, A. F. Morabito, S. C. Pavone, N. I. Piazzese, L. Di Donato, T. Isernia, and G. Sorbello, "Compact circularly polarized array for direction finding: Use of conventional steering vector versus embedded radiation patterns," in *Proc. 17th Eur. Conf. Antennas Propag. (EuCAP)*, Mar. 2023, pp. 1–5.

[23] O. Crisafulli and A. F. Morabito, "Wideband circular polarized microstrip antenna for direction of arrival applications," in *Proc. 24th Riunione Nazionale di Elettromagnetismo (RiNEm)*, 2022, pp. 1–5.

[24] C. A. Di Carlo, L. Di Donato, G. S. Mauro, R. La Rosa, P. Livreri, and G. Sorbello, "A circularly polarized wideband high gain patch antenna for wireless power transfer," *Microw. Opt. Technol. Lett.*, vol. 60, no. 3, pp. 620–625, Mar. 2018.

[25] G. Kumar, V. Gupta, and R. Tank, "Phase-based angle estimation approach in indoor localization system using Bluetooth low energy," in *Proc. Int. Conf. Smart Electron. Commun. (ICOSEC)*, Sep. 2020, pp. 904–912.

[26] M. Malajner, K. Benkic, P. Planinsic, and Z. Cucej, "The accuracy of propagation models for distance measurement between WSN nodes," in *Proc. 16th Int. Conf. Syst., Signals Image Process.*, Jun. 2009, pp. 1–4.

[27] S. J. Orfanidis, *Electromagnetic Waves and Antennas*, 2016. [Online]. Available: https://www.ece.rutgers.edu/~orfanidi/ewa/

[28] H. Krim and M. Viberg, "Two decades of array signal processing research: The parametric approach," *IEEE Signal Process. Mag.*, vol. 13, no. 4, pp. 67–94, Jul. 1996.

[29] W. Zhao, J.-K. Zhang, X.-P. Zhang, and R. Zheng, "Multiple-target localization by millimeter-wave radars with trapezoid virtual antenna arrays," *IEEE Internet Things J.*, vol. 9, no. 20, pp. 19589–19598, Oct. 2022.

OTTAVIO CRISAFULLI received the bachelor's degree in informatics engineering and the master's degree in communications engineering from the University of Catania, Italy. He is currently pursuing the Ph.D. degree with the Department of Information Engineering, Infrastructure, and Sustainable Energy, Mediterranean University of Reggio, Italy. His master's thesis was on the monitoring and prediction models of the electromagnetic field levels at the base station. His research interests include antenna and array antenna design for direction-finding applications and the study of algorithms to estimate the direction of arrival of both coherent and non-coherent signals.

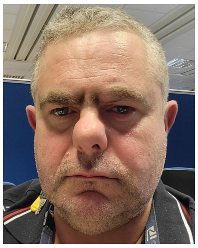

NICOLÒ IVAN PIAZZESE was born in Acireale, Catania, Italy, in 1972. He received the degree in electronic engineering from the University of Catania, Italy, in 1999. He joined STMicroelectronics Catania, in 2000. He started working in CDMA and OFDM receivers, i.e., 3GPP HSDPA and 802.11b devices. From 2005 to 2008, he worked on the design of UWB radar algorithms. From 2009 to 2022, he has designed algorithms for ISM band transceivers. His research interests include digital filter design, modeling techniques of analog and mixed-signal systems, and spectral analysis applied to direction-finding algorithms.

SANTI CONCETTO PAVONE (Senior Member, IEEE) received the B.Sc. and M.Sc. degrees (cum laude) in electronics engineering from the University of Messina, Italy, in 2010 and 2012, respectively, and the Ph.D. degree (Doctor Europaeus) in information engineering and science from the University of Siena, Italy, in 2015, with a focus on electromagnetics engineering. He was a Visiting Ph.D. Student and a Visiting Assistant Professor with Institut d'Électronique et de Télécommunications de Rennes (IETR), Rennes, France, in 2015 and 2020, respectively. From July 2016 to July 2019, he was an Associate Researcher with the Laboratory of Applied Electromagnetics, University of Siena. From 2019 to 2023, he has been an Assistant Professor with DIEEI, University of Catania, Italy, where he has been a Senior Assistant Professor (RTD-B), since October 2023. His current research interests include electromagnetic theory, scattering theory, RADAR design at millimeter waves, high-frequency techniques, focusing systems, non-diffractive localized pulses, and reconfigurable antennas. He was a recipient of the ESF Research Networking Program "NEWFOCUS" Scholarship, in 2015, and the IEEE AP-S Student Award granted by the AP-S/MTT-S Chapter Central-Southern Italy, in 2014. In 2017, he was a Finalist for the Best Paper Award in Electromagnetics and Antenna Theory at the 11th European Conference on Antennas and Propagation (EuCAP), Paris. In 2018, he was a co-recipient of the Best Paper Award in Electromagnetics and Antenna Theory at the 12th EuCAP, London. In 2020, he got Italian Scientific Habilitation for Associate Professorship of Electromagnetic Fields. In 2020, 2021, 2022, and 2023, he was selected among outstanding reviewers of IEEE TRANSACTIONS ON ANTENNAS AND PROPAGATION. In 2019, 2021, and 2022, he was a recipient of the Young Scientist Awards at the 41st Progress in Electromagnetics Research Symposium, Rome, the XXXIV General Assembly and Scientific Symposium of the International Union of Radio Science, Rome, and the Third Atlantic Asia–Pacific Radio Science Meeting, Gran Canaria, Spain. He serves as an Associate Editor for IEEE ACCESS, *IET Electronics Letters*, and *Frontiers in Antennas and Propagation*.

GIUSEPPE GIAMMELLO received the M.Sc. degree in automation engineering from the University of Catania, in 2018. He is currently pursuing the Ph.D. degree with Dipartimento di Ingegneria Elettrica, Elettronica ed Informatica (DIEEI), University of Catania, while collaborating with INGV-OE. He has been a Research Fellow with Istituto Nazionale di Geofisica e Vulcanologia, Osservatorio Etneo (INGV-OE) for two years, contributing to the remote sensing of volcanic phenomena. His research interests include signal processing of radar data and remote sensing.

GIOVANNI GALVAGNA received the bachelor's degree in electronic engineering and the master's degree in automation engineering and control of complex systems from the University of Catania, in 2015 and 2018, respectively. During this period, he joined the INFN-LNS as a Scholarship Recipient, providing technical support to the department's activities, such as PCB design, software, and firmware development. He joined STMicroelectronics Catania, in 2021, as a Radio Frequency Application Engineer for products at 2.4 GHz and SubGHz bands. He is making contributions to the design and development of antenna arrays for AoA/AoD solutions.

SALVATORE PITRULLI received the bachelor's degree (cum laude) in computer and telecommunications engineering from Messina University, in 2007, and the master's degree (cum laude) in telecommunications engineering from Catania University, in 2010. He began his career at STMicroelectronics Catania, in 2010, as an Application Engineer of RF products, especially on microcontrollers using Bluetooth low-energy technology. His current research interest includes firmware development.

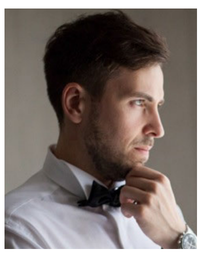

ANDREA FRANCESCO MORABITO (Senior Member, IEEE) received the Ph.D. degree in computer, biomedical, and telecommunications engineering and the Laurea degree (summa cum laude) in telecommunications engineering from the Mediterranean University of Reggio Calabria, Italy. He is currently an Associate Professor of electromagnetic fields with the Mediterranean University of Reggio Calabria. He has coauthored more than 100 scientific papers in international peer-review journals and conference proceedings. His research interests include models and effective strategies for the solution of inverse problems in electromagnetics, including inverse scattering, phase retrieval, antenna synthesis, and theranostics problems with applications ranging from biomedical imaging and microwave hyperthermia to radar, 5G, and satellite telecommunications. He has been awarded by Italian Electromagnetics Society with both the Barzilai and Latmiral Prizes.

LORETO DI DONATO (Senior Member, IEEE) received the M.Sc. and B.Sc. (Laurea) degrees in biomedical engineering from the University of Naples "Federico II," Italy, in 2006 and 2008, respectively, and the Ph.D. degree in information engineering (applied electromagnetics) from the University "Mediterranea" of Reggio di Calabria, in 2012. In 2009, he joined the Electromagnetic Diagnostic Research Group, Institute for Electromagnetic Sensing of the Environment—National Research Council (IREA-CNR) of Italy, Naples, with a study and research grant. Since 2013, he has been with the Department of Electrical, Electronics and Computer Engineering, where he was an Assistant Professor, from 2013 to 2019, and has been an Associate Professor of electromagnetic fields, since 2021. His research interests include inverse scattering problems, antenna synthesis problems, and bioelectromagnetic interactions at millimeter waves. He was a Young Scientist at the XXXIII International Conference on Ground Penetrating Radar, in 2010; the Young Scientist Awarded at the XXX URSI General Assembly, in 2011; the Honorable Mention from the IEEE Antennas and Propagation Society Committee (Chapter Central and Southern Italy) in a Student Member Best Paper Competition, in 2012; and "Gaetano Latmiral" Prize from Societã Italiana di Elettromagnetismo, in 2016.

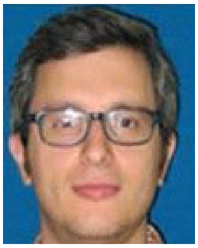

MICHELE SARDO received the master's degree from Pisa University, in 1993. His master's thesis was on parallel computation architectures. After that, he started working in the industry with Hewlett and Packard on parallel architectures. Then, he joined STMicroelectronics Catania, where he worked in several technologies, including embedded firmware, embedded Linux, IEEE 802.15.4 technology, ZigBee, and RF protocols development. Lately, he has been responsible for applications on low-power low-data-rate RF products for subGHz and Bluetooth low-energy.

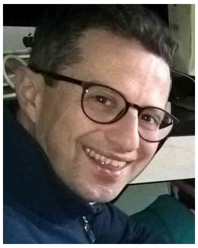

GINO SORBELLO (Member, IEEE) received the Laurea degree (cum laude) in electronics engineering from the University of Catania, Catania, Italy, in 1996, and the Ph.D. degree in electronics and communications engineering from the Polytechnic Institute of Milan, Milan, Italy, in 2000. He was an Assistant Professor of electromagnetic fields with the University of Catania, in 2002, where he has been an Associate Professor of electromagnetic fields with the Department of Electrical, Electronics, and Computer Engineering, since 2014. Since 2012, he has been a member of INFN-LNS and collaborates with the Ion Sources and Plasma Physics Group. His current research interests include planar antenna development, including ultra-wideband antennas and compact antennas, antenna synthesis and inverse problems, the study of microwave devices and computational electromagnetism, single-mode solid-state waveguide lasers and optical amplifiers, integrated optics, RF-plasma interactions, and particle accelerators.

Open Access funding provided by 'Università degli Studi di Catania' within the CRUI CARE Agreement